Restricted Dynamics in Poly(ether ether ketone) As Revealed by Incoherent Quasielastic Neutron Scattering and Broad-Band Dielectric Spectroscopy

A. Nogales,[†] T. A. Ezquerra,*[,†] F. Batallán,[‡] B. Frick,[§] E. López-Cabarcos,[||] and F. J. Baltá-Calleja[†]

Instituto de Estructura de la Materia, CSIC, Serrano 119, Madrid 28006, Spain, Instituto de Ciencia de Materiales de Madrid, CSIC, Cantoblanco, Madrid 28049, Spain, Institut Laue-Langevin, 38042 Grenoble Cedex, France, and Deptartamento Química-Física II, Facultad de Farmacia, Universidad Complutense, Madrid 28040, Spain

Received October 7, 1998; Revised Manuscript Received December 15, 1998

ABSTRACT: The molecular dynamics of semicrystalline poly(ether ether ketone) (PEEK) was studied over a broad dynamic range from 10^{-1} to 10^{9} Hz by combining dielectric spectroscopy (DS) and incoherent quasielastic neutron scattering (IQNS). This allowed us to characterize the polymer dynamics in the glassy, semicrystalline, and molten states. By performing dielectric and neutron-scattering measurements in a comparable frequency range, we proved that the quasielastic broadening observed in IQNS experiments corresponds to the dielectric α relaxation without invoking any kind of low-frequency dielectric data extrapolation. IQNS measurements indicate that the segmental chain motion observed at temperatures higher than the glass transition temperature possesses an elastic and a quasielastic contribution. A model which considers a confined-jump diffusive motion allows a quantitative description of the IQNS spectra. This model provides dimensions of jump length, residence time, available space, and number of scatterers involved in the process. Results indicate that both the size of the restricted volume and the amount of protons involved in the α process increase with temperature and are smaller than the calculated values based on the crystallinity estimates from calorimetric and X-ray diffraction experiments. Both effects indicate for semicrystalline PEEK the existence of a confined amorphous phase with regions of different degrees of mobility. The present experiments provide a quantitative dynamical and spatial description of the heterogeneous amorphous phase of semicrystalline PEEK.

1. Introduction

The microstructure of semicrystalline polymers typically displays a distinct morphology consisting of laminar crystals intercalated by less ordered regions. The distribution of the crystalline regions may give rise to the appearance of different textures.[1] It is known that the dynamics of the amorphous phase in semicrystalline polymers presents characteristic features which differ from those observed in pure amorphous polymers.[2] In particular, at temperatures higher than the glass transition temperature (T_g), polymer chain segments in the amorphous regions are restricted to move between the crystals.[2,3] This confinement broadens the glass transition region and shifts T_g toward higher values.[4] Above T_g, the confinement effects are reflected in the dielectric α relaxation provoking a decrease of the dielectric strength, an increase of the central relaxation time, τ, and a broadening of the relaxation process.[2,3,5] The dynamics of the amorphous phase in a semicrystalline polymer can be envisioned as a result of a process of self-confinement within the restricted geometry imposed by the crystalline regions as crystallinity develops. A strong interaction between the amorphous phase and the crystalline interphase is expected as polymer chains in the former are physically connected with the crystals. Relaxation and calorimetric experiments performed on semicrystalline polymers reveal the existence, above T_g, of different levels of mobility in the amorphous regions. In particular, the existence of a rigid amorphous phase (RAP) which does not relax or only relaxes partially well above T_g has been proposed.[6−11] The location of the RAP in the crystal−amorphous interphase or as an independent phase still is an open question.

In addition to dynamic mechanical analysis and dielectric spectroscopy, incoherent-neutron-scattering experiments are valuable when one deals with polymer dynamics. On one hand, the possibility of measuring the energy transfer between the neutron and the polymer allows one to study polymer dynamics above and below T_g. On the other, from the dependence of the incoherent scattered intensity on the momentum transfer (Q), information about the geometrical characteristics and length scale of the molecular motion can be inferred.[12,13]

Poly(ether ether ketone)[14] (PEEK) is a semirigid polymer which can be crystallized either from the melt or from the glassy state. PEEK has been extensively studied, and it is known that its crystals are arranged in a spherulitic morphology when crystallized from the melt or from the glassy state at temperatures lower than 573 K.[15−17] Spherulites consist of dense lamellar stacks of crystals and amorphous pockets or gaps between and within them.[15,18] The existence of a rigid amorphous phase in this polymer has been demonstrated by means of several techniques.[9,10,19,20] However, there is still some controversy about the degree of mobility of the RAP in the range between T_g and T_m.[9,10] Dielectric experiments have shown an increase of the dielectric strength of the α relaxation[10] with temperature pointing toward a progressive mobilization of the RAP.

[†] Instituto de Estructura de la Materia, C.S.I.C.
[‡] Instituto de Ciencia de Materiales de Madrid, C.S.I.C.
[§] Institut Laue-Langevin.
[||] Universidad Complutense.

10.1021/ma9815758 CCC: $18.00
Published on Web 03/16/1999

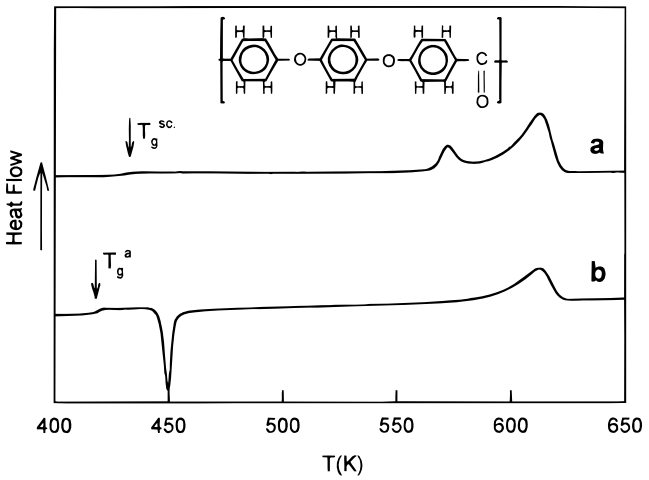

Figure 1. DSC scans of initially semicrystalline (a) and amorphous (b) PEEK. Heating rate: 20 K/min.

In the present study, the relaxation process of the amorphous phase of PEEK confined within its own crystals is analyzed over a broad dynamic range above T_g by combining dielectric spectroscopy and incoherent quasielastic neutron scattering (IQNS). The aim of this work is to present a quantitative dynamical and spatial description of the heterogeneous amorphous phase of semicrystalline PEEK.

2. Experimental Section

2.1. Materials. The polymer investigated was PEEK 450 G from ICI in the form of amorphous films with a thickness of $\approx 50\ \mu$m. This sample has a number-average molecular weight of $M_n = 15\ 200$ and a weight-average molecular weight of $M_w = 40\ 000$. The glass transition temperature of the amorphous sample, as measured by differential scanning calorimetry (DSC), is 418 K. The chemical structure of the repeating unit is shown in the inset of Figure 1.

2.2. Techniques. DSC experiments were carried out with a Perkin-Elmer DSC7 instrument at a heating rate of 20 K/min. The temperature was calibrated by using indium and zinc standards. The samples were encapsulated in aluminum pans, and the typical sample weights used in these experiments were about 7 mg.

Measurements of the complex dielectric permittivity, $\epsilon^* = \epsilon' - i\epsilon''$, were performed over a broad frequency window, 10^{-1} Hz $< F < 10^8$ Hz, in a temperature range of 123 K $< T <$ 423 K. To cover the above frequency range, three different experimental setups were used. From 10^{-1} to 10^5 Hz a Novocontrol system integrating an SR 830 lock-in amplifier with a dielectric interface was employed. In the range 10^6-10^8 Hz, dielectric measurements were obtained by means of an HP 4291 coaxial line reflectometer. In this case, the complex permittivity was calculated by measuring the reflection coefficient at a particular reference plane.[21] These two instruments were integrated in a Novocontrol broad-band dielectric spectrometer. The temperature in this spectrometer is controlled by a nitrogen jet with a temperature error, during every single sweep in frequency, of ± 0.1 K. The frequency gap from 10^5 to 10^6 Hz was covered by using an HP 4192 impedance analyzer. Dielectric measurements in this frequency range were performed by using a home-made cryostat operating under a temperature-controlled nitrogen atmosphere. Owing to the fact that two different cryostats were used, the measuring temperatures do not completely coincide. To obtain the whole isothermal curve, the ϵ'' values in the 10^5-10^6 Hz range were interpolated between two consecutive isothermal measurements performed with the HP 4192. Circular gold electrodes were sputtered onto the free surfaces of the films with diameters of 3 cm for the measurements up to 10^6 Hz and 0.5 cm for measurements at $F > 10^6$ Hz.

The phenomenological Havriliak−Negami (HN)[22] formulation was used to describe the dielectric α relaxation. In this approach, the complex dielectric permittivity exhibits a frequency (ω) dependence of the form

$$\epsilon^* = \epsilon_\infty + \frac{\epsilon_0 - \epsilon_\infty}{[1 + (i\omega\tau_0)^b]^c} \tag{1}$$

where ϵ_0 and ϵ_∞ are the relaxed ($\omega = 0$) and unrelaxed ($\omega = \infty$) dielectric constant values, τ_0 is the central relaxation time of the relaxation time distribution function, and b and c [$0 < (b, c) < 1$] are shape parameters which describe the symmetric and the asymmetric broadening of the relaxation time distribution function, respectively.[22] Equation 1 leads to a Debye single relaxation time equation when $b = c = 1$. In semicrystalline polymers, there appears an enhanced contribution to ϵ'' at low frequencies which is attributed to the polarization of the crystal surface.[2] Therefore, to analyze the shape and temperature evolution of the α relaxation, a conduction term was included in eq 1 as $\sigma/(\epsilon_{vac}\omega^s)$, were σ is related to the direct current electrical conductivity, ϵ_{vac} is the vacuum dielectric constant, and s is related to the nature of the conduction mechanism. A value of $s < 1$ is related to a non-ohmic transport.[23]

Neutron-scattering measurements were carried out on the neutron backscattering spectrometer IN10, at the Institute Laue-Langevin (ILL) in Grenoble, France. This spectrometer allows one to look for dynamics around 10^{-9} s. The incident neutron wavelength was $\lambda = 6.27$ Å. The experimental Q range of the instrument was 0.4 Å$^{-1} < Q <$ 2.0 Å^{-1} where Q is the momentum transfer defined by $Q = (4\pi/\lambda)\sin(\theta)$, 2θ being the scattering angle. Two series of measurements were performed at several Q vectors covering the whole Q range of the instrument. In the first series, a temperature range between 4 and 400 K was covered by using a cryofurnace. In the second series, a range between 300 and 700 K was covered using a furnace. The quasielastic measurements were performed by varying the monochromator position with a mechanical Doppler driver which provides an experimental energy window of $-14\ \mu$eV $< E < 14\ \mu$eV. Quasielastic spectra were recorded at selected temperatures for every Q. Accumulation times of 12 h for $T <$ 550 K and 24 h for $T >$ 550 K were typically used. The samples were either hollow cylinders of 3 cm diameter or flat square specimens (3×4 cm^2). The thickness of the sample was selected to yield a transmission of about 90%. The experimental resolution was obtained from a measurement performed at 4 K, where it was assumed that no molecular motion occurs. Standard correction programs of ILL were used to subtract the scattering from those of the empty cell and spectrometer and to correct for detector and analyzer efficiency, as well as for self-screening and absorption of the sample.

The incoherent-scattering cross section of hydrogen is very large in comparison with the coherent- and incoherent-scattering cross sections of other atoms such as carbon and oxygen. Accordingly, for PEEK, the ratio between σ_{inc} for hydrogen and the total scattering cross section, σ_t, is about 0.87. Thus, measurement of the incoherent-scattering function for the hydrogen atoms of the polymer provides information about the dynamics of the polymeric chains. For the analysis of our experimental data, we consider the molecular motion formed by the combination of a vibrational motion and a relaxation process. In this case, assuming that the vibrational and the relaxation motions are uncoupled and provided that the inelastic contribution appears well separated from the quasielastic one, the incoherent scattering function $S_{inc}(Q, \omega)$ can be described by[12,24,25]

$$S_{inc}(Q, \omega) = S_{inc}^{vib}(Q, \omega) \otimes S_{inc}^{rel}(Q, \omega) \tag{2}$$

where $\otimes$ means the convolution product in ω and $S_{inc}^{vib}(Q, \omega)$ is the incoherent-scattering function of the vibrational motion which corresponds to the elastic Debye−Waller factor. For the

relaxation process, the quasielastic function $S_{inc}^{rel}(Q, \omega)$ is given by a quasielastic contribution and an elastic component in the following way:

$$S_{inc}^{rel}(Q, \omega) = A_0(Q)\,\delta(\omega) + [1 - A_0(Q)]\,L(\omega, \Gamma(Q)) \quad (3)$$

where $L(\omega, \Gamma(Q))$ is a relaxation function with a half-width at half-maximum (HWHM) $\Gamma(Q)$ and $A_0(Q)$ is the elastic-incoherent-scattering function (EISF). For the data treatment, a convolution of $S_{inc}(Q, \omega)$ with the experimental resolution was made. From the fit with the experimental results, $A_0(Q)$ and $L(\omega, \Gamma(Q))$ were obtained. In a second step, more specific models for the Q-dependence of $A_0(Q)$ and $\Gamma(Q)$ were proposed to obtain the geometrical parameters of the dynamics.

3. Results

3.1. Differential Scanning Calorimetry. Figure 1 shows the DSC traces of a semicrystalline PEEK specimen (a) and an amorphous PEEK film (b). The glass transition for the amorphous sample manifests itself by a jump in the heat flow at $T_g = 418$ K. When the sample is heated at 20 K/min, a sharp exotherm appears, indicating the cold crystallization of amorphous PEEK. The crystallization temperature measured at the minimum of the exotherm is 448 K. At higher temperatures, an endothermic peak centered around 613 K evidences the melting of the PEEK crystals. The thermal history of the semicrystalline sample was chosen to reproduce the one followed in the IQNS experiments. The sample was crystallized from the glassy state by heating at 1.5 K/min, in three temperature steps of 50 K starting at 400 K (450, 500, and 550 K, respectively). At each temperature, the sample was held isothermally for 7 h. After the final treatment at 550 K, the sample was cooled to room temperature. The corresponding DSC experiment of this sample (trace a, Figure 1) shows a shift toward higher values of the T_g and a smaller jump at the glass transition as compared with the amorphous one. The magnitude of this jump is proportional to the amount of material which relaxes at the glass transition defined by $X_a = (\Delta C_p)^{sc}/(\Delta C_p)^a$. Here, $(\Delta C_p)^{sc}$ and $(\Delta C_p)^a$ are the heat capacity increments at T_g for the semicrystalline and amorphous samples, respectively. At higher temperature, two endothermic peaks are present which correspond to the melting of two populations of crystal lamellae. The low-temperature peak can be associated with the melting of secondary lamellae while the high-temperature endotherm is attributed to the melting of primary lamellae.[15] The amount of crystalline material, X_c, can be calculated from the area of the melting endotherm assuming for the melting enthalpy of the 100% crystalline PEEK a value of 130 J/g.[26] According to previous studies of this polymer,[9] ΔC_p is not exclusively proportional to the amorphous weight fraction $(1 - X_c)$. The amount of amorphous material which remains immobile beyond the glass transition temperature (X_{RAP}) can be estimated from the ΔC_p measurement by $X_{RAP} = 1 - X_c - X_a$. In our case, for the semicrystalline sample, values of $X_c \approx 0.34 \pm 0.01$, $X_a \approx 0.48 \pm 0.06$, and then $X_{RAP} \approx 0.18 \pm 0.07$ are derived. These values are in qualitative agreement with previously reported values.[9]

3.2. Broad-Band Dielectric Spectroscopy. The dielectric loss values, ϵ'', of a semicrystalline PEEK sample are presented as a function of frequency for several temperatures in Figure 2a. The thermal history of the semicrystalline sample was the same as that described in section 3.1 (trace a in Figure 1). In the investigated temperature range ($T > T_g$), the α relaxation appears as a maximum in ϵ'' which is accompanied by a strong increase of ϵ'' at lower frequencies. The frequency of maximum loss F_{max} shifts toward higher values as temperature increases. For the sake of comparison, dielectric loss values of an amorphous PEEK sample are presented in Figure 2b. In this case, the values of ϵ'' are higher than those obtained for the semicrystalline sample. The relaxation peaks are centered around 10^4 Hz at $T = 433$ K for the amorphous sample and at 453 K for the semicrystalline sample. This indicates that a displacement of the α relaxation toward higher temperatures takes place when the sample is semicrystalline. It is to be noted that while the intensity of the relaxation peak decreases with increasing temperature for the amorphous sample, the opposite trend is found for the semicrystalline one.

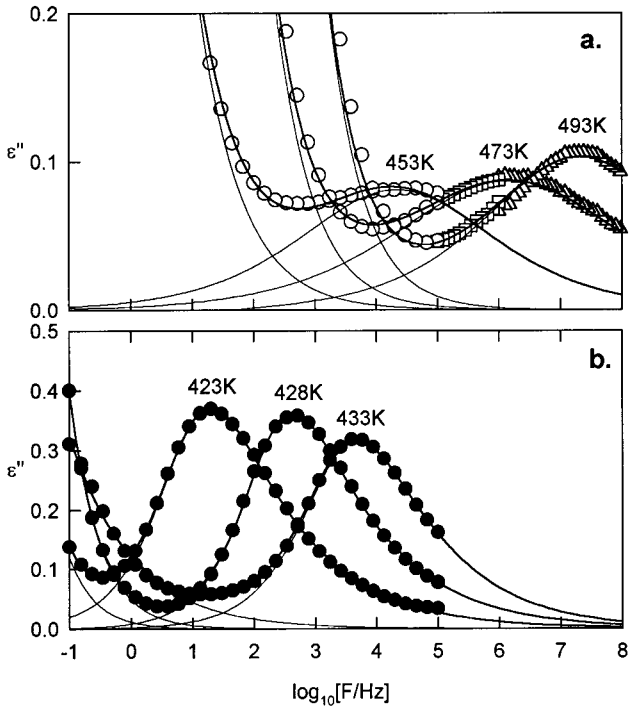

Figure 2. Dielectric loss values, ϵ'', for semicrystalline (a) and amorphous (b) PEEK. Different symbols represent the three different spectrometers used (see Experimental Section). Lines represent best fits according to eq 1. Thinner lines represent the separate contributions of the conduction and relaxation processes.

The α relaxation is attributed to segmental motions of the polymer chains appearing at temperatures higher than T_g. The strong increase of ϵ'' at low frequencies is due to the contribution of the electrical conductivity. At each temperature, ϵ'' values for both the semicrystalline and amorphous samples were fitted according to eq 1, and the result of this treatment is presented in Figure 2 by the continuous lines. The separate contributions of both the relaxation and the conduction processes are represented. From the analysis of the experimental dielectric curves, the characteristic parameters of eq 1 such as $\Delta\epsilon = \epsilon_0 - \epsilon_\infty$, b, c, τ_0, σ, and s are obtained. Tables 1 and 2 summarize these values for the experimental results of Figure 2. In Figure 3, the F_{max} values for the semicrystalline sample are represented as a function of the reciprocal temperature. The dependence of F_{max} on temperature clearly exhibits a non-Arrhenius behavior. A Vogel−Fulcher−Tamann (VFT) function of

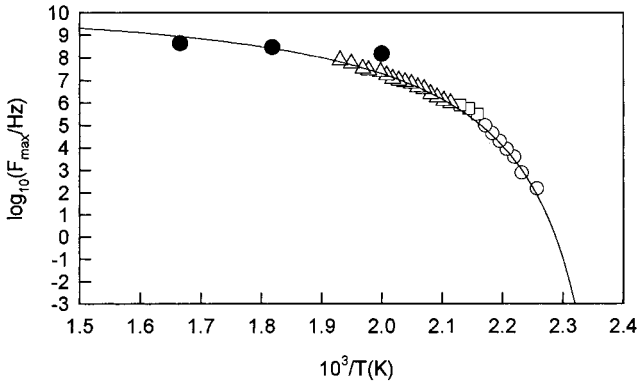

Figure 3. Frequency of maximum loss, F_{max}, values as a function of reciprocal temperature (open symbols). Different symbols represent data obtained by using different spectrometers. Full symbols represent the equivalent frequency ($F = 1/(2\pi\tau)$) obtained from the IQNS data. The continuous line represents the best fit of the experimental data to the VFT equation.

Table 1. $\Delta\epsilon$, b, τ_0, σ, and s Values Obtained from the Fitting of Eq 1 in the Case of the α Relaxation of the Semicrystalline Sample

T (°C)	$\Delta\epsilon$	b	τ_0 (s)	σ	s
443	0.53	0.33	2.2×10^{-4}	5.8×10^{-12}	0.59
453	0.53	0.38	7.4×10^{-6}	2.7×10^{-11}	0.62
473	0.57	0.36	1.1×10^{-7}	3.6×10^{-10}	0.72
483	0.61	0.39	2.5×10^{-8}	9.0×10^{-11}	0.73
493	0.62	0.41	7.5×10^{-9}	1.5×10^{-9}	0.73

Table 2. $\Delta\epsilon$, b, c, τ_0, σ, and s Values Obtained from the Fitting of Eq 1 in the Case of the α Relaxation of the Amorphous Sample

T (°C)	$\Delta\epsilon$	b	c	τ_0 (s)	σ	s
423	1.50	0.78	0.46	1.9×10^{-2}	6.7×10^{-13}	0.99
428	1.42	0.82	0.44	8.7×10^{-4}	2.31×10^{-12}	0.90
433	1.29	0.72	0.53	7.1×10^{-5}	2.35×10^{-12}	0.56

the type

$$F_{max} = F_0 \exp\left(\frac{-A}{T - T_0}\right) \quad (4)$$

can satisfactorily describe the experimental results with the following parameters: A = 648.7 K, T_0 = 410 K, and $F_0 = 2.7 \times 10^{10}$ Hz.

3.3. Incoherent Quasielastic Neutron Scattering. Incoherent-quasielastic-neutron-scattering (IQNS) experiments were performed at selected temperatures in the range from 300 to 650 K. Figure 4 shows IQNS spectra for the highest measured Q (1.95 Å^{-1}) at different temperatures. The experimental data are represented by circles. For temperatures below 450 K, no quasielastic broadening can be detected and the quasielastic scattered intensity falls into the experimental resolution of the spectrometer. At these temperatures, the experimental data can be fitted simply by a $\delta(\omega)$ function. As temperature increases, the quasielastic component appears. In the temperature range 500−600 K, the data can be fitted to a model function consisting of the sum of a $\delta(\omega)$ and a Lorentzian function (eq 3). The continuous curves represent the best fit according to this model function where the separated contributions of both the δ functions and the Lorentzian curves convoluted with the experimental resolution are presented. The Q-structure of this quasielastic broadening is shown in Figure 5, where IQNS spectra are

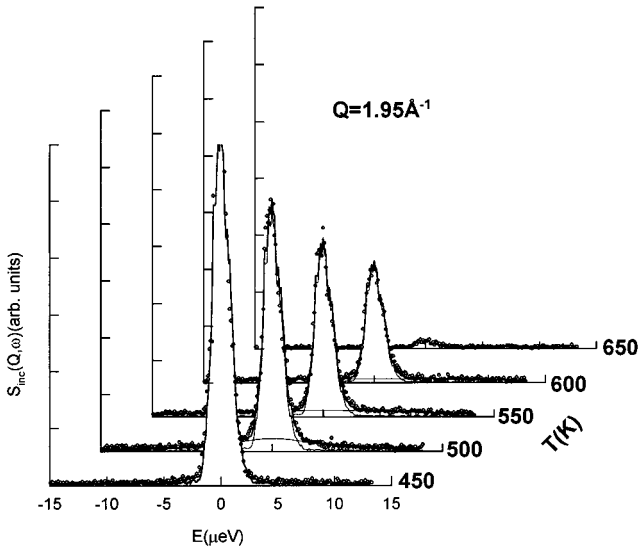

Figure 4. Quasielastic-neutron-scattering spectra as a function of temperature for $Q = 1.95$ Å^{-1}: (○) experimental points; (—) experimental resolution, Lorentzian curve, and best fit according to eq 3.

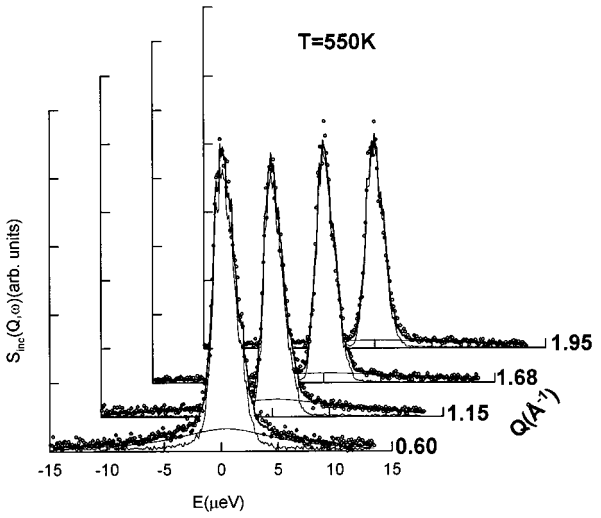

Figure 5. Quasielastic-neutron-scattering spectra for four selected Q values at $T = 550$ K. Same symbols as in Figure 4.

represented at a fixed temperature (T = 550 K) for different Q values. An increase of the quasielastic broadening and a decrease of the height with the Q vector are observed.

From the analysis of each quasielastic spectrum according to eq 3, two functions can be extracted: (a) the elastic-incoherent-scattering-function (EISF), defined by $A_0(Q)$ in eq 3, and (b) the half-width at half-maximum of the Lorentzian function ($\Gamma(Q)$). Figure 6 shows $A_0(Q)$ and $\Gamma(Q)$ as functions of Q obtained for the four spectra at temperatures above 450 K. As one can see, A_0 values initially decrease with increasing Q and finally tend to constant values. In the molten state, T = 650 K, only the low-Q spectra present small evidence of an elastic component while, for $Q > 0.5$ Å^{-1}, $A_0(Q) = 0$. Figure 6b shows $\Gamma(Q)$ as a function of Q for the measured temperatures. For the highest measured temperatures, in the molten state, a large part of the signal is no longer within the observation window and $\Gamma(Q)$ is only accessible for $Q < 0.5$ Å^{-1}.

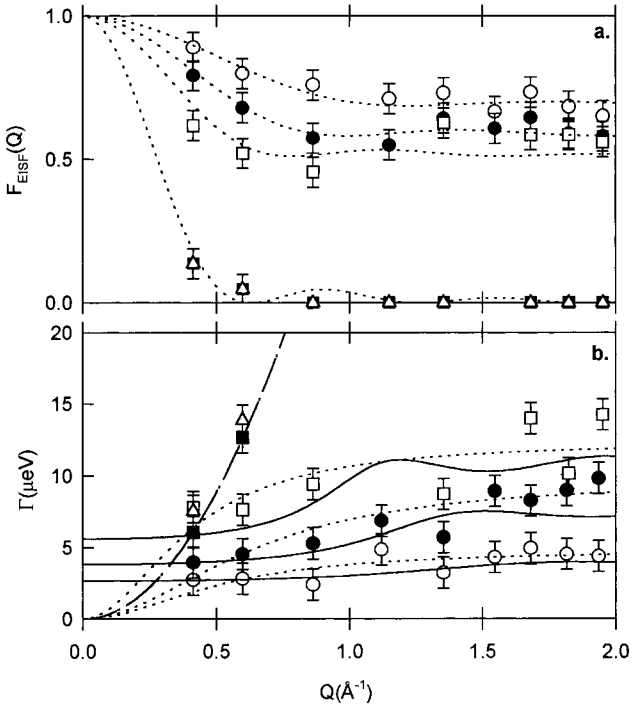

Figure 6. (a) Elastic-incoherent-scattering factor, EISF, and (b) Γ(Q) as a function of Q at different temperatures: ○, 500 K; ●, 550 K; □, 600 K; ■, 630 K; △, 650 K. Dotted lines represent the best fit of the experimental points to a jump diffusion model. Continuous lines in (b) correspond to a jump diffusion model in a restricted volume. Dashed lines are guides for the eye.

4. Discussion

4.1. IQNS: Jump Diffusion within a Restricted Volume. IQNS measurements (Figures 4 and 5) indicate the existence of a molecular motion with an elastic and a quasielastic contribution. The existence of an elastic component, provided by the EISF values shown in Figure 6a, is both temperature- and Q-dependent. This is characteristic of a motion taking place within a restricted geometry.[24,27−29] In this case, the EISF, $A_0(Q)$, is the Fourier transform of the restricted volume[24,25] while the Q dependence of $A_0(Q)$ contains the geometrical parameters of the volume.

It is well-known that in polymers there are entanglements which restrict the free motion of a polymer chain.[30] Because of this, polymer chains exhibit a certain degree of confinement imposed by the presence of the neighbour chains. Quasielastic-neutron-scattering experiments have provided evidence of this restricted dynamics and have provided information about the size of the confinement range.[31] In another approach, it has been proposed that relaxation in glass-forming liquids takes place in cooperatively rearranging regions (CRR).[32,33] The size of these domains diverges as T_g is approached from higher temperatures.[32] Experimental techniques including dielectric spectroscopy,[34] calorimetry,[33] light scattering,[35] and X-ray scattering[36] have shown that the sizes of these domains may range from 7 to about 22 Å at T_g depending on the system. According to this, the ability of the jump diffusion model in a restricted volume to describe our experiments is not surprising if one considers that the volume which can be explored by the proton is strongly restricted by two factors: (i) the above-mentioned interaction with neighbouring chains that restricts the available space and (ii) the presence of crystals which restrict the availability of spatial conformations.

Table 3. r_0, τ, L, and n Values Obtained from the Analysis of the EISF and the HWHM (Γ(Q))

T (K)	r_0 (Å)	τ (s)	L (Å)	n
500	2.4	1.4×10^{-9}	5.1	0.3
550	2.4	5.3×10^{-10}	6.4	0.4
600	2.9	3.6×10^{-10}	8.0	0.5
650			10	1

Usually, the EISF depends on geometrical factors but not on temperature.[24] However, in our case, EISF exhibits a clear temperature dependence (Figure 6a). A temperature dependence of the EISF has been observed in polymeric samples with certain levels of order[29,37] suggesting the existence of protons with different dynamics in the sample. NMR experiments also may provide information about the existence of different levels of mobility in the amorphous phase of semicrystalline polymers,[6−8] including PEEK.[38] The simplest approach to account for this finding within the model is to consider two kinds of proton scatterers: a fraction $n(T)$ contributing to a jump diffusion motion in a restricted volume and the rest, $1 - n(T)$, remaining immobile. The fraction of immobile protons must be understood as those protons with mobility well below the lower limit of the dynamic range of the spectrometer. Hence, eq 3 could be rewritten as

$$S_{inc}(Q, \omega) = n(T)\{A_0(Q)\,\delta(\omega) + [1 - A_0(Q)]L(\omega, \Gamma(Q))\} + [1 - n(T)]\delta(\omega) \quad (5)$$

The observed EISF could then be described by the function

$$F_{EISF}(T, Q) = n(T)[A_0(Q) - 1] + 1 \quad (6)$$

The simplest case of diffusion within a restricted region is the one-dimensional diffusion of a particle between two rigid and impermeable boundaries. Considering that the two boundaries are separated by a distance L, the elastic structure factor is given by[27]

$$A_0(Q) = j_0^2(QL/2) \quad (7)$$

where j_0 is the spherical Bessel function of the first kind and zero order. A fit of the experimental F_{EISF} values to equations 6 and 7 is presented in Figure 6a by the dotted lines. For 630 and 650 K, in the molten state, F_{EISF} values tend to zero as Q increases according to eq 7. This indicates that all the proton scatterers are in motion; i.e., eq 6 is strictly valid with $n(T) = 1$. From the fittings of F_{EISF} to the experimental results, the values for L and $n(T)$ have been extracted (see Table 3). Figure 7 presents these values as a function of temperature. As one can see, the magnitudes, of both $n(T)$ and L increase nearly linearly with temperature until the melting temperature. The rise of $n(T)$ with temperature indicates a progressive mobilization of initially immobilized protons. The separation into mobile and immobile protons is just a first approximation to the problem. Physically, there should be a distribution of temperature-activated mobilities. In this context, the increment of $n(T)$ can be interpreted as an increase in the number of mobile units with $\tau \approx 10^{-9}$ s. In the molten state, no variation of the number of proton scatterers with temperature is observed because all the protons are expected to be in motion and therefore $n(T)$

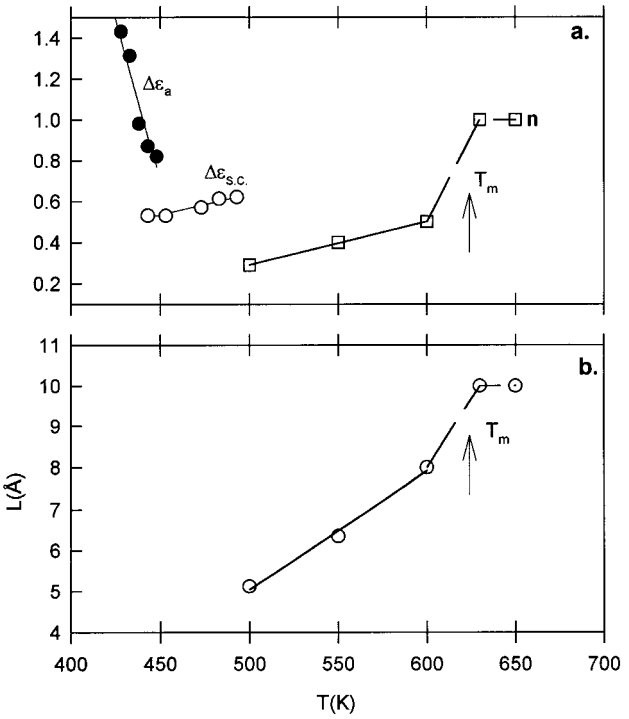

Figure 7. (a) Temperature dependence of $\Delta\epsilon$ calculated from dielectric spectroscopy for the amorphous (●) and semicrystalline samples (○) and $n(T)$ calculated from IQNS experiments (□). (b) L, characteristic length of the restricted volume calculated from IQNS experiments.

= 1. Since the temperature range covered by us is 212 K > ($T - T_g$) > 32 K, the absolute values of 5 Å < L < 10 Å are within the considerations of the CRR scheme.

The experimental values of $\Gamma(Q)$ (figure 6b) show an asymptotic behavior at high Q-vectors. This finding indicates that this motion is not a simple continuous diffusion because, in this case, a $\Gamma(Q) = D_{diff}Q^2$ behavior, where D_{diff} is the diffusion constant, should be expected.[25] An asymptotic behavior at large Q for $\Gamma(Q)$ can be obtained by considering that diffusion takes place by means of a jumping mechanism between different sites.[27] In this model, the characteristic parameters are the jump length, r_0, and the residence time τ. If one considers a Gaussian distribution of jump lengths, the experimental data of Figure 6b can be analyzed by using the expression[27]

$$\Gamma(Q) = \frac{1}{\tau}\left[1 - \exp\left(-\frac{Q^2 r_0^2}{2}\right)\right] \qquad (8)$$

In Figure 6b, the fitting of this equation to the experimental values is shown by the dotted curves. From this fitting, a value for the characteristic jump parameter $r_0 \approx 2.5 \pm 0.4$ Å is obtained. The corresponding values for the residence time τ (see Table 3) have been represented in Figure 3 as a function of the reciprocal temperature.

It is noteworthy that the previous analysis of EISF assumes that the motion takes place in a restricted volume with a characteristic parameter $L(T)$. However, the model for $\Gamma(Q)$ described in eq 8 predicts that $\Gamma(0) = 0$ for $Q = 0$, which is characteristic of a motion occurring within an infinite volume. The existence of a restricted volume modifies the $\Gamma(Q)$ behavior at low Q, especially in the range between 0 and $2\pi/L$.[27] Volino and co-workers[28] studied a continuous diffusion in a restricted volume of given geometrical shapes. Hall and Ross[27] calculated the one-dimensional case of the spatially bounded random jump in a volume limited by two boundaries assuming a Gaussian distribution of jump lengths. The asymptotic value ($Q \rightarrow 0$) for both models is the same. The model found for $S_{inc}(Q, \omega)$ follows:

$$S_{inc}(Q, \omega) = A_0(QL)\,\delta(\omega) + \sum_{n=1}^{\infty} A_n(QL)\,L(\omega, \Gamma_n(QL)) \qquad (9)$$

This equation consists of (i) an elastic component, a $\delta(\omega)$ function with an amplitude A_0(QL) (eq 7), and (ii) a quasielastic component, an infinite series of Lorentzian functions $L(\omega, \Gamma_n(QL))$, each one with amplitude $A_n(QL)$ given by

$$A_n(QL) = \frac{(2QL)^2}{[(QL)^2 - (n\pi)^2]^2}[1 - (-1)^n \cos(QL)] \qquad (10)$$

The HWHM, $\Gamma(QL)$, of the Lorentzian functions $L(\omega, \Gamma_n)$ is expressed by

$$\Gamma_n(QL) = \frac{1}{\tau}\left[1 - \exp\left(\frac{-n^2\pi^2 r_0^2}{2L^2}\right)\right] \qquad (11)$$

where again r_0^2 is the mean-square jump length and τ is the residence time between two successive jumps. In this model, the width of each Lorentzian function is independent of Q. The Q dependence of the infinite sum of eq 9 comes from the amplitudes A_n.

The parameters of this model are τ, L, and r_0. Taking the values of Table 3 for these parameters, we calculated $S_{inc}(Q, \omega)$ according to eq 9. Forty terms of the series were taken into account. The resulting quasielastic contribution can be fitted to a single Lorentzian function with a Q-dependent width considered as the HWHM. Considering that A_n decreases as $1/n^4$ for fixed QL,[27] the series converges rapidly. Calculations considering more terms do not modify the HWHM values.

The resulting HWHM values as a function of Q calculated at three temperatures for the semicrystalline sample are shown in Figure 6 as continuous curves. As seen, the model describes the trend of the experimental data within the error of measurement. Moreover, at low Q values, the large-range characteristics of the motion are observed. Therefore, the effect of the boundaries is reflected in the experiments by $\Gamma(Q) \neq 0$. Indeed, by comparing $\Gamma(Q)$ obtained either from the jump diffusion in an infinite-volume model (dotted line in Figure 6) or from the jump diffusion in a restricted-volume model (continuous line in Figure 6), one observes that the stronger differences appear in the low-Q region for $Q << 2\pi/L$. The limited Q range prevents us from giving a more accurate description in the low-Q region.

4.2. Molecular Origin of the Quasielastic Broadening. The obtained values for both r_0 and L can be interpreted by considering that the proton−proton distance in the phenyl ring is about 4.3 Å.Thus the calculated L values are in agreement with a motion of the proton in an effective space larger than that defined by a flip of the phenyl ring. Here, the elementary jumps, characterized by r_0, can be associated with a motion of the proton around its covalent bond. The L variation with temperature (Figure 7b) indicates that the motion not only is just a simple flip or rotation of the benzene ring but also involves a certain degree of translation.

In support of this, it is to be noted that localized benzene motions are typically faster than those investigated by the IN10 spectrometer and frequently appear in the millielectronvolt energy range.[12,39] Moreover, upon comparison of the loss of elastic intensity with temperature with the first appearance of quasielastic broadening, it seems that there must be a quasielastic contribution, probably from a localized motion, at a higher frequency scale, i.e. a higher energy range than that covered by us.[40] Hence, we can attribute the quasielastic broadening appearing in the measured temperature and Q ranges to the α relaxation process. Dielectric spectroscopy measurements reveal the existence of a molecular motion in the investigated temperature range which is attributed to the segmental motions giving rise to the α relaxation (Figure 2).[10,19] Due to the broad frequency band used in the dielectric spectroscopy experiments, F_{max} values can be directly compared with the corresponding ones derived from the IQNS experiments considering that $F_{IQNS} = 1/(2\pi\tau)$. In Figure 3 both F_{max} from the dielectric experiments and F_{IQNS} values are represented.

A VFT behavior is observed for the F_{max} values as expected for the α relaxation process. The absolute values of F_{max} and F_{IQNS} differ by about 1 order of magnitude at 500 K and tend to merge at higher temperatures, approaching the calculated VFT curve. The differences of the absolute values as measured by the two different techniques can be attributed to the different molecular probes used in both techniques. The molecular probe in the dielectric experiments is the dipole moment of the ketone, ether, and benzene groups while in the IQNS experiments it is the protons attached to the phenyl rings. Consequently, IQNS experiments reveal the contribution of the phenyl rings to the α relaxation while dielectric experiments show up the overall segmental motion. The good overlap of IQNS and DS in Figure 3 suggests that the same relaxation process is being observed by both techniques.

4.3. Influence of Crystallinity on the Dynamics. Dielectric experiments performed in both amorphous and semicrystalline PEEK above T_g reveal a temperature dependence of τ corresponding to the α relaxation strongly deviating from an Arrhenius behavior. The strong−fragile scheme proposed by Angell[41] allows one to classify glass-forming liquids on the basis of the temperature dependence exhibited by the corresponding relaxation times (τ). By scaling τ-values as a function of T_g/T, we can compare the relaxation time temperature dependences of systems with different T_g values. Within this scheme, the fragility of a system is defined as the degree of departure from the Arrhenius behavior exhibited by the relaxation time of the α relaxation process.[41] The parameter A from the VFT equation (eq 4) can be replaced by DT_0 where D is the strength parameter.[41] In polymers, fragility has been associated with the strength of the correlation between nonbonded species and has been renamed cooperativity.[42]

In Figure 8 we have replotted the F_{max} data of Figure 3 as a cooperativity plot (τ vs T_g/T). The dielectric relaxation time, τ, has been calculated according to $\tau = 1/(2\pi F_{max})$. For the sake of comparison, PEEK dielectric data taken from the literature[10] have been included. The characteristic τ values calculated by IQNS experiments were taken from Table 3. Data for amorphous and semicrystalline PEEK were normalized to the calorimetric T_g value (Figure 1). Although semicrystalline and amorphous samples exhibit different T_g values, upon scaling by T_g/T, we see that τ values tend to collapse into a single curve, in agreement with previous experiments and theroretical predictions.[42]

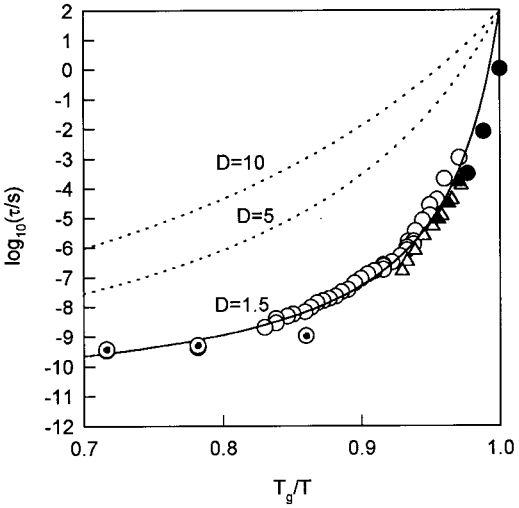

Figure 8. Cooperativity plot: τ versus T_g/T for PEEK. T_g is the calorimetric glass transition temperature. Full symbols correspond to amorphous PEEK and empty symbols to semicrystalline PEEK: △, ref 10; and ○, this work; ⊙, IQNS data. The dotted lines correspond to several strength parameters D. The continuous line represents the best fit to the data according to the VFT equation.]

It is evident that the α relaxation times for PEEK strongly deviate from an Arrhenius behavior which would correspond to a straight line in this plot. This effect is quantified by a small value of the strength parameter ($D = 1.5$). This value is smaller than the reported values for other polymers including benzene rings in the backbone, such as poly(ethylene terephthalate) (PET) and the polycarbonate from bisphenol A (BPA-PC).[41,43] This could be attributed to the higher rigidity of the chain structure of PEEK as compared with PET and BPA-PC. It is noteworthy that the least fragile polymer reported exhibits a value of $D = 16$ (polyisobutylene).[44]

Owing to the existence of crystallinity, in the semicrystalline sample the α relaxation appears as a symmetric ($c = 1$) and relatively broad process (low b values, Table 1). In contrast to what happens in amorphous PEEK, the dielectric strength, $\Delta\epsilon$, for the semicrystalline sample increases with temperature (Table 1, Figure 7a). This effect has been previously reported for semicrystalline PEEK samples.[10,19] According to the Kirkwood−Fröhlich equation,[3] in a first approximation, the dielectric strength is directly proportional to the amount of dipoles involved in the relaxation and inversely proportional to the temperature as shown by

$$\Delta\epsilon \propto \frac{N}{T} g(T)\, \mu^2(T) \qquad (12)$$

where N is the number of dipoles, μ is the effective dipole moment, and g is the correlation factor which contains contributions of both inter- and intrachain dipolar correlations. The $\Delta\epsilon$ increases with temperature can be attributed to a progressive mobilization of dipoles involved in the relaxation, giving rise to a temperature dependence of N.[10,19] In semicrystalline polymers, the dipoles included in the crystals are at fixed positions and cannot contribute to the α relaxation process. It has

been proposed that a given part of the dipoles is included in a rigid amorphous phase (RAP) whose mobility increases with temperature.[10,19] This means that the material belonging to the RAP does not contribute to the overall crystallinity because it is in a disordered region though it can relax depending on temperature.[10] In our case, evidence for the existence of the RAP has been derived not only from the DSC experiments (Figure 1), which at T_g give for the RAP a value of 0.18, but also from the IQNS experiments. Since the crystallinity of PEEK in our experiments is $X_c \approx 0.34$ one observes that the fraction of immobile material derived from IQNS experiments, $1 - n(T)$, is also higher than that expected only on the basis of the crystalline material. Moreover, our present results confirm the existence of an RAP when the measured $\Delta\epsilon$ values, in our case, are compared with the amount of mobile protons, $n(T)$, as derived by IQNS experiments (Figure 7). Both magnitudes increase similarly with temperature. As the magnitudes of both $\Delta\epsilon$ and n provide information about the amount of mobile material, the progressive incorporation of a fraction of initially immobile material into the relaxation process, as temperature increases, seems to be confirmed by two different techniques.

A final remark should be made about the physical meaning of the restricted volume in our case. Results presented in Figure 7 indicate that L increases with temperature up to the melting point and then remains constant. By comparing L values for the semicrystalline and molten samples (Figure 7b), we observe the restrictions in the dynamics imposed by the crystals as a decrease in the size of L. The facts that the L values are much smaller than the size of the calculated amorphous layer (≈50 Å)[15] and that L decreases with decreasing temperature favors the existence of a rigid amorphous phase whose mobility increases with temperature. Further experiments extended to higher dynamic and temperature ranges are necessary to shed light on this point.

5. Conclusions

By a combination of dielectric spectroscopy (DS) and incoherent quasielastic neutron scattering (IQNS), the molecular dynamics of semicrystalline poly(ether ether ketone) (PEEK) could be studied in the glassy, semicrystalline, and molten states. It is shown that the origin of the quasielastic broadening observed in the IQNS spectra for $T > 450$ K is the α relaxation process which manifests itself as a maximum in the imaginary part of the complex dielectric permittivity (ϵ^*). The motion observed by IQNS experiments has been described as a jump diffusion process taking place within a restricted volume whose size gradually varies with temperature from $L = 5$ Å to $L = 8$ Å in the semicrystalline sample and discontinuously increases to 10 Å near the melting point. The analysis of the IQNS spectra indicates (i) that the amount of mobile protons is smaller than that calculated on the exclusive basis of the DSC crystallinity and (ii) that the amount rises with temperature. Similarly, the amount of mobile dipoles estimated from $\Delta\epsilon$ for the semicrystalline specimen shows an increase with temperature. The above effects support the existence, in semicrystalline polymers, of a confined amorphous phase with regions of different degrees of mobility.

References and Notes

(1) Zachmann, H. G.; Wutz, C. In *Crystallization of Polymers*; Dosière, M., Ed.; Kluwer Academic Publishers: Dordrecht, The Netherlands, 1993; p 403.
(2) Coburn, J. C.; Boyd, R. H. *Macromolecules* **1986**, *19*, 2238.
(3) Williams, G. In *Structure and Properties of Polymers*; Cahn, H. W., Haasen, P., Kramer, E. J., Eds.; Materials Science and Technology, Vol. 12; VCH: Weinheim, Germany, 1993.
(4) Wunderlich, B. *Prog. Colloid Polym. Sci.* **1994**, *96*, 22.
(5) Ezquerra, T. A.; Majszczyk, J.; Baltá-Calleja, F. J.; López-Cabarcos, E.; Gardner, K. H.; Hsiao, B. S. *Phys. Rev. B* **1994**, *50*, 6023.
(6) Axelson, D. E. In *High Resolution NMR Spectroscopy of Synthetic Polymers in Bulk*; Komoroski, R. A., Ed.; VCH: Weinheim, Germany, 1986.
(7) Dörlitz, H.; Zachmann, H. G. *J. Macromol. Sci., Phys.* **1997**, *B36*, 205.
(8) Abis, L.; Floridi, G.; Merlo, E.; Pò, R.; Zannoni, C. *J. Polym. Sci.: Part B: Polym. Phys.* **1998**, *36*, 1557.
(9) Cheng, S. Z. D.; Cao, M. Y.; Wunderlich, B. *Macromolecules* **1986**, *19*, 1868.
(10) Huo, P.; Cebe, P. *Macromolecules* **1992**, *25*, 902.
(11) Sauer, B. B.; Hsiao, B. S. *Polymer* **1995**, *36*, 2553.
(12) Higgings, J. S.; Benoit, H. *Polymers and Neutron Scattering*; Clarendon Press: Oxford, U.K., 1994.
(13) Colmenero, J.; Arbe, A.; Alegria, A. *Phys. Rev. Lett.* **1993**, *71*, 2603.
(14) Poly(ether ether ketone) is the customary name of poly(oxy-1,4-phenyleneoxy-1,4-phenylenecarbonyl-1,4-phenylene).
(15) Verma, R.; Marand, H.; Hsiao, B. S. *Macromolecules* **1996**, *29*, 7767.
(16) Basset, D. C.; Olley, R. H.; Al Raheil, I. A. M. *Polymer* **1988**, *29*, 1945.
(17) Marand, H.; Prasad, A. *Macromolecules* **1992**, *25*, 1731.
(18) Jonas, A. M.; Russell, T. P.; Yoon, D. Y. *Colloid Polym. Sci.* **1994**, *272*, 1344.
(19) Kalika, D. S.; Krishnaswamy, R. K. *Macromolecules* **1993**, *26*, 4252.
(20) Jonas, A.; Legras, R. *Macromolecules* **1993**, *26*, 813.
(21) Ezquerra, T. A.; Kremer, F.; Wegner, G. In *Dielectric Properties of Heterogeneous Materials*; Priou, A., Ed.; Progress in Electromagnetic Research, Vol. 6; Elsevier: Amsterdam, 1992; Chapter 7.
(22) Havriliak, S.; Negami, S. *Polymer* **1967**, *8*, 161.
(23) Kirst, K. U.; Kremer, F.; Litvinov, V. M. *Macromolecules* **1993**, *26*, 975.
(24) Beé, M. *Quasielastic Neutron Scattering. Principles and Applications*; A. Hilger: Bristol, U.K., 1988.
(25) Springer, T. *Quasielastic Neutron Scattering for the Investigation of Diffusive Motions in Solids and Liquids*; Springer: Berlin, 1972.
(26) Blundell, D. J.; Osborn, B. N. *Polymer* **1983**, *24*, 953.
(27) Hall, P. L.; Ross, D. K. *Mol. Phys.* **1981**, *42*, 673.
(28) Volino, F.; Dianoux, A. J. *Mol. Phys.* **1980**, *41*, 271.
(29) Lecommandoux, S.; Dianoux, A. J.; Hardouin, F. *ILL-Annual Report*; ILL: Grenoble, France, 1995; p 386.
(30) Strobl, G. *The Physics of Polymers*; Springer Verlag: Berlin, 1996; p 277.
(31) Richter, D.; Farago, B.; Fetters, L. J.; Huang, J. S.; Ewen, B.; Lartigue, C. *Phys. Rev. Lett.* **1990**, *64*, 1389.
(32) Adam, G.; Gibbs, J. H. *J. Chem. Phys.* **1965**, *43*, 139.
(33) Donth, E. *J. Non-Cryst. Solids* **1982**, *53*, 325.
(34) Dobbertin, J.; Hensel, A.; Schick, C. *J. Therm. Anal.* **1996**, *47*, 1027.
(35) Fischer, E. W.; Donth, E.; Steffen, W. *Phys. Rev. Lett.* **1992**, *68*, 2344.
(36) Moynihan, C. T.; Schroeder, J. *J. Non-Cryst. Solids* **1993**, *160*, 52.
(37) López-Cabarcos, E.; Batallán, F.; Frick, B.; Ezquerra, T. A.; Baltá-Calleja, F. J. *Phys. Rev. B* **1994**, *50*, 13214.
(38) Poliks, M. D.; Schaefer, *J. Macromolecules* **1990**, *23*, 3426.
(39) Koizumi, S. *J. Chem. Phys.* **1997**, *107*, 603.
(40) Ezquerra, T. A.; Nogales, A.; Batallán, F.; Frick, B. *ILL-Annual Report*; ILL: Grenoble, France, 1996; p 382.
(41) Böhmer, R.; Ngai, K. L.; Angell, C. A.; Plazek, D. J. *J. Chem. Phys.* **1993**, *99*, 4201.
(42) Ngai, K. L.; Roland, C. M. *Macromolecules* **1993**, *26*, 2688.
(43) Ngai, K. L.; Roland, C. M. *Macromolecules* **1993**, *26*, 6824.
(44) Frick, B.; Richter, D. *Phys. Rev. B* **1993**, *47*, 14795.

MA9815758